Journal of Porous Materials (2022) 29:1369–1383
https://doi.org/10.1007/s10934-022-01262-w

Functionalized diatom biosilica decorated with nanoparticles: synthesis, characterization, catalytic oxidation, and dye scavenging applications

Parimal Pandit[1] · Pranita Rananaware[1] · Aviva D'Souza[1] · Mahaveer D. Kurkuri[2] · Varsha Brahmkhatri[1]

Accepted: 2 May 2022 / Published online: 20 May 2022

Abstract

Diatoms are unicellular photosynthetic algae that occur in all water territories on earth. Their cell walls comprise amorphous siliceous material, biosilica, called a frustule. Attributable to their highly porous structure, diatom biosilica is a promising renewable material for various applications such as catalysis, drug delivery systems, adsorbents, and biophotonics. In the current work, to enhance the properties of diatoms (*Aulocoseira sp.*), they were surface-functionalized with thiol groups and decorated with silver or gold nanoparticles. Comprising diatoms biosilica (DE) as catalyst support with Nobel metal nanoparticles as active species, the two series of catalysts, DE-SH-AuNP and DE-SH-AgNP, were synthesized. The material was characterized by various spectroscopic techniques such as SEM-EDAX, BET surface area, FT-IR, XRD, TEM, ^{29}Si-NMR, and TGA-DTA analysis. With a homogeneous nanoparticle distribution, diatom biosilica exhibited very high nanoparticle-loading (AgNP and AuNP) capacities. The synthesized catalysts DE-SH-AuNP and DE-SH-AgNP were investigated for oxidation of D-glucose to D-gluconic acid, an essential chemical intermediate in the pharmaceutical and food industry. Additionally, the catalysts were also investigated for environmental applications like dye degradation studies for methylene blue (MB) and crystal violet (CV) using UV–visible spectroscopy. The catalysts exhibited excellent activity for the oxidation of D-glucose with 78% conversion over DE-XSH-Ag and 87% conversion over DE-XSH-Au respectively. The preliminary results of dye degradation studies reveal the potential of materials in environmental applications.

Keywords Diatoms · Gold nanoparticles · Silver nanoparticles · Glucose oxidation · Dye degradation

Abbreviations

AuNP	Gold nanoparticles.
AgNP	Silver nanoparticles.
DE	Diatoms biosilica.
MB	methylene blue.
CV	crystal violet.
CY	chrysoidine Y.
X	xerogel.
MTPMS	3-mercaptopropyltrimethoxysilane.
TEOS	Tetraethoxysilane.
FESEM	Field emission scanning electron microscope.
EDAX	Energy-dispersive X-ray spectroscopy.
TEM	Transmission electron microscope.
BET	Brunauer-Emmett-Teller.
AT-IR	Attenuated total reflectance infrared spectra.
XRD	X-ray diffraction.
TGA-DTA	Thermogravimetric Analysis-Differential thermal analysis.
JCPDS	Joint Committee on Powder Diffraction Standards.
NMR	Nuclear Magnetic resonance.

✉ Mahaveer D. Kurkuri
mahaveer.kurkuri@jainuniversity.ac.in

✉ Varsha Brahmkhatri
b.varsha@jainuniversity.ac.in

[1] Centre for Nano and Material Sciences, Jain University, Jain Global Campus, 562112 Bengaluru, Karnataka, India

[2] Centre for Research in Functional Materials (CRFM), Jain University, Jain Global Campus, 562112 Bengaluru, Karnataka, India

1 Introduction

Diatomite, a white mineral powder obtained from the mining industry, is pure diatom frustules known as biosilica(Saxena et al. 2022). They stand out different among all the reported biomaterials as they demonstrate the highest strength-to-weight ratio(Aitken et al. 2016; Moreno et al. 2015), and intense light absorption ability(Prins et al. 2020). They have a unique 3D porous structure that provides exceptional chemical, catalytic, photonic, and absorptive properties, making them promising applicants in nanotechnology applications (Dolatabadi and de la Guardia 2011; Korsunsky et al. 2020; Panwar and Dutta 2019; Rabiee et al. 2021; Shelar et al. 2021; Uthappa et al. 2018b). However, biosilica is an inert material integrally(Gholami et al. 2020; Mishra et al. 2017), which significantly limits many potential applications and advancements in making new composite materials using them. Subsequently, considerable efforts have been made to modify diatom silica using various methods like surface functionalization and making composites with other materials like metal oxides(Esfandyari et al. 2020; Maeda et al. 2018), metal-organic frameworks(Liu et al. 2014; Uthappa et al. 2020), polymers(Feng et al. 2016), and enzymes(Bayramoglu et al. 2013; Kim et al. 2020; Leonardo et al. 2016).

Recently the surface modification of diatoms to tailor the preferred surface functional groups that enhance the surface properties is getting tremendous interest(De Stefano et al. 2008; Delasoie and Zobi 2019). Additionally, the surface modification method involved silane modification(Gutiérrez Moreno et al. 2020; Kucuk et al. 2020), xerogel (Uthappa et al. 2018a, 2019), and ceria(Sriram et al. 2020) modification for diverse applications. Another promising surface modification of diatoms is the decoration with various metal nanoparticles like Au, Ag, and Pt (Briceño et al. 2021; Jantschke et al. 2012; Sherief et al. 2021; Uthappa et al. 2019; Vona et al. 2018). To date, various diatoms species have been explored for surface decoration with nanoparticles to enhance their activities(Su et al. 2018). Fischer et al. reported for the first time that three different species of diatoms *Stephanopyxis turris, Eucampia zodiacus*, and *Thalassiosira pseudonana* were used as catalyst support for gold nanoparticles synthesized by the covalent coupling method. They report ex-situ decoration of AuNPs on diatom surfaces. Initially, the surface of diatoms was modified with APTMS followed by ex-situ covalent coupling of the nanoparticle by NHS/EDC chemistry(Fischer et al. 2016). This method requires additional steps for the decoration of nanoparticle surfaces. Gupta et al. reported the *in-situ* synthesis of AgNPs on diatoms by peptide-mediated photo-reduction

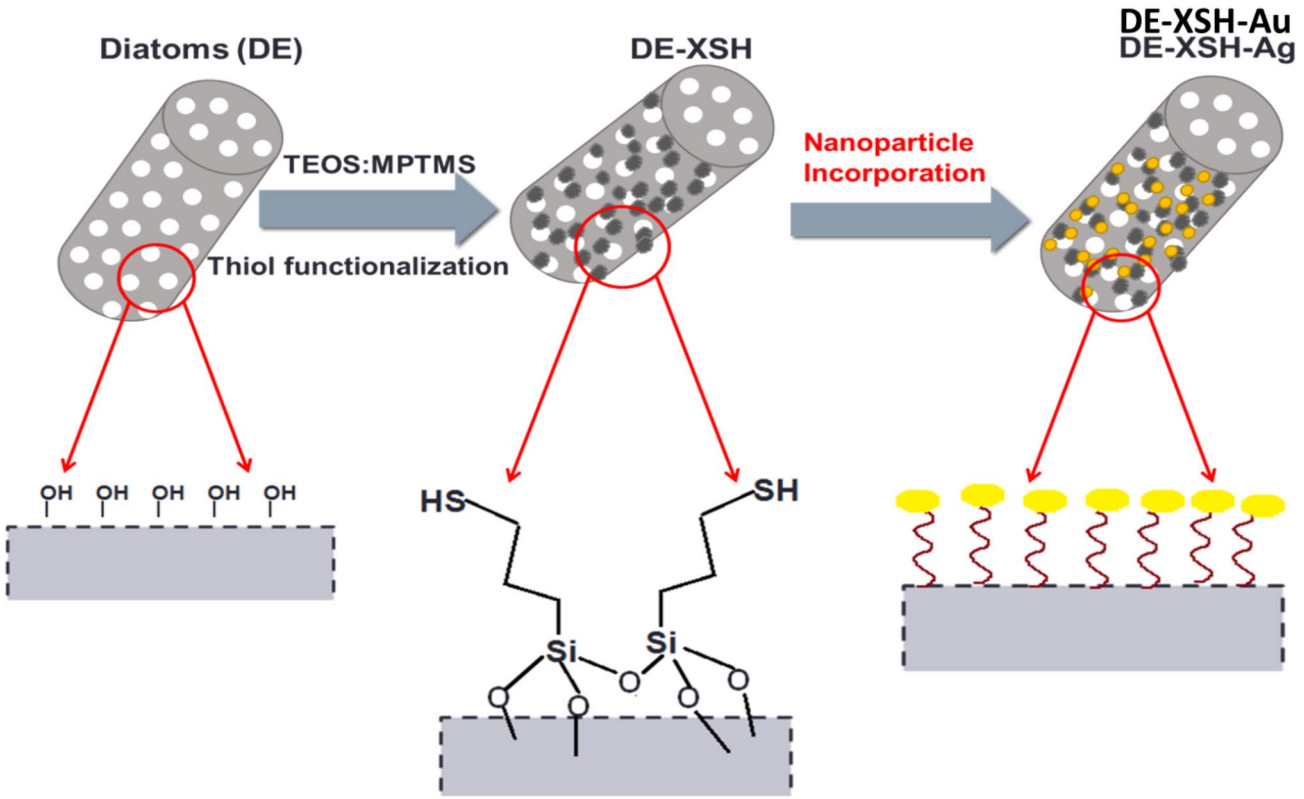

Scheme 1 Gold and Silver nanoparticle decorated diatom silica catalysts

method, and the resulting nanocomposite was used in dye synthesized solar cells for energy applications(Gupta et al. 2018). Chetia and the group reported that the diatom species *Navicula* from Asam was used for silver nanoparticle surface modification. The AgNPs on the diatom surface were decorated in *in-situ* in the presence of light. The resulting composite was used for sensing applications to detect dissolved ammonia at room temperature(Chetia et al. 2017).

The diatom silica decorated with different nanoparticle are reported earlier, and previous attempts show that they were used in varied applications like catalysis, sensing, drug delivery, and energy applications(Abukhadra et al. 2019; Della Rosa et al. 2019; Kamińska et al. 2017; Onesto et al. 2018). The main significance and highlights of this work are the decoration of diatom silica surface by Nobel metal nanoparticles, AuNP and AgNP. These nanoparticles find applications in various fields like catalysis and

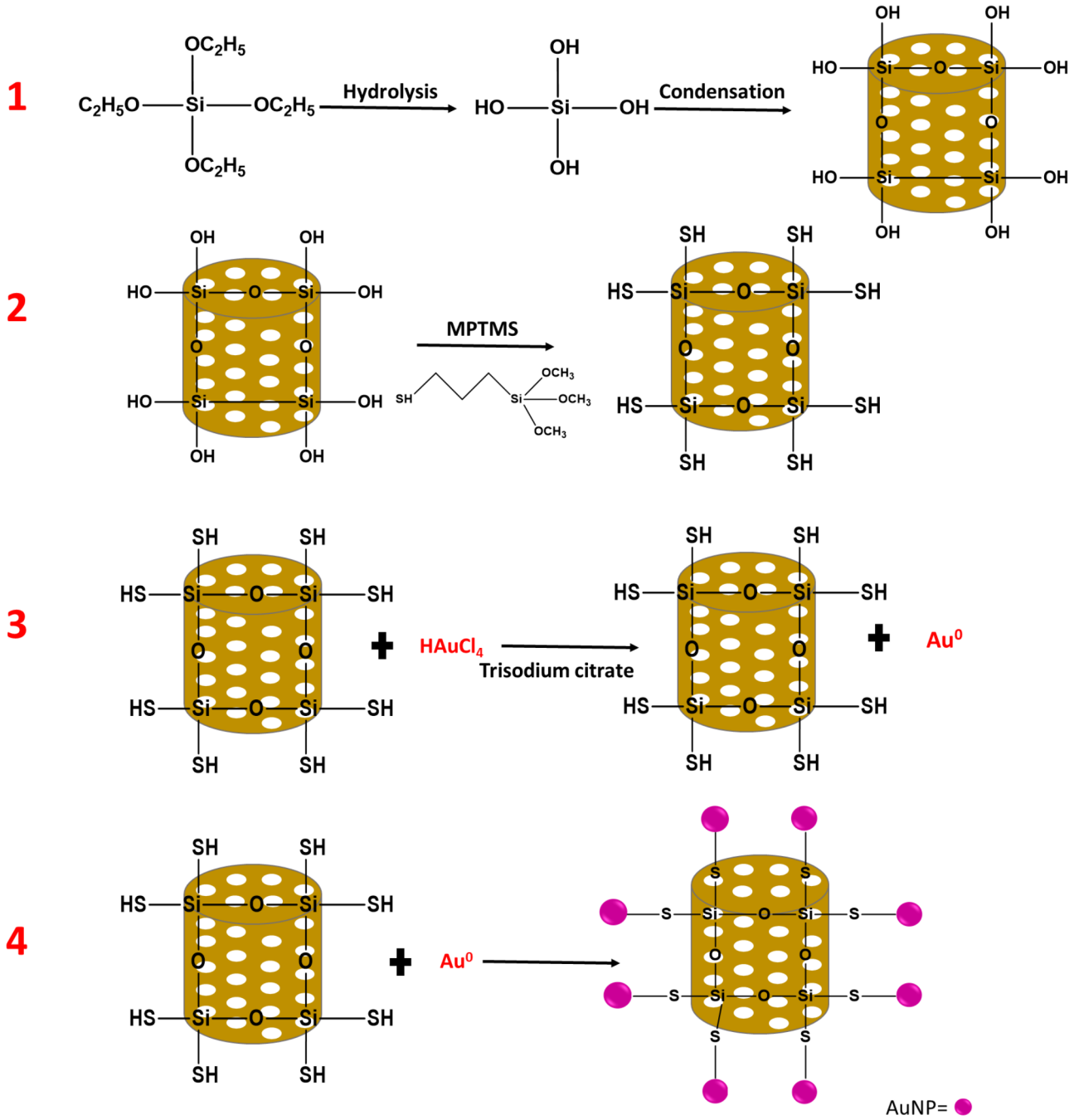

Scheme 2 Chemical reactions showing oxidation/reduction taking place for the in-situ nanoparticle synthesis (AuNP/AgNP)

sensing(Brahmkhatri et al. 2021). Herein, the diatom surface is first functionalized with MTPMS, leading to –SH functional groups on the surface. This is followed by *in-situ* nanoparticle synthesis (gold or silver), wherein nanoparticles are conjugated through –SH groups on the diatom surface via formation of Au-S, Ag-S bonds. This approach enables the uniform, well - dispersed nanoparticles on diatom surfaces and escapes the leaching problems from the surface of diatoms. As an application, these catalysts were investigated for catalytic oxidation of D- Glucose and for environmental application, evaluated for dye degradation signifying them as multifunctional heterogeneous catalysts.

The principal strategy to synthesize nanoparticles is the *in-situ* reduction process of metal precursors on the diatom surface using sodium borohydride $NaBH_4$. The e*x-situ* methods suffer from the use of multiple and complicated steps; hence the preferably *in-situ* method is generally followed(Briceño et al. 2021). The current studies report natural planktonic *Aulacoseira* diatoms functionalized with –SH group, decorated with gold or silver nanoparticles *via in-situ* method wherein metal nanoparticle precursors $HAuCl_4$ and $AgNO_3$ were reduced using sodium borohydride as shown in Scheme 1.

Additionally, the chemical reactions to depict oxidation/reduction taking place for the in-situ nanoparticle synthesis (gold or silver) over diatom surface are shown in Scheme 2. The resulting materials were explored for oxidation of glucose and dye degradation applications. The bare diatoms, surface-functionalized and nanoparticle-decorated catalysts were characterized by FT-IR, XRD, SEM, TEM, BET, and ^{29}Si MAS-NMR. To the best of our knowledge, decoration of diatoms by nanoparticles (AuNP and AgNP) via an organic linker by the *in-situ* method has not been reported previously.

2 Experimental and characterization

2.1 Materials and methods

DE was obtained from Mount Sylvia (Australia) Pvt. Ltd., All the chemicals and analytical grade reagents and solvents were used as received. Tetraethoxysilane (TEOS) (Cas No.- 78-10-4), 3-mercaptopropyltrimethoxysilane (MPTMS) (Cas No.- 4420-74-0), $HAuCl_4$ (Cas No.- 16903-35-8), $AgNO_3$ (Cas No.- 7761-88-8), and D-Glucose (Cas No.- 50-99-7) were procured from Sigma-Aldrich (India) Pvt. Ltd. Hydrochloric acid (HCl) (Cas No.- 7647-01-0), ammonia (NH3) (Cas No.- 7664-41-7), ethanol (Cas No.- 64-17-5), methylene blue(Cas No.- 61-73-4), and Chrysoidine Y (Cas No.- 532-82-1) were obtained from NICE chemicals (India) Pvt. Ltd. Sodium citrate (Cas No.- 6132-04-3), sodium borohydrite (Cas No.- 16940-66-2) were obtained from s.d.fine chemicals.

2.2 Synthesis of thiol functionalized diatom silica (DE-XSH)

The DE was purified according to the previously reported method(Şan et al. 2009). The surface modification of DE with xerogel is well studied and reported earlier by our group(Uthappa et al. 2018a). Presently the surface modification of DE with xerogel(X) and thiol(-SH) Functionalization was done together in one step. In brief, 250 mg of DE was taken in a beaker, dispersed with 2 mL of double distilled water, and stirred for a minute. Further, dropwise added 2 mL TEOS as a precursor of silica xerogel and 333µL of MPTMS for thiol functionalization. At this stage 0.5 mL of conc. HCL was added to the above mixture. The gel formation was done by dropwise addition of 0.5 to 2 mL ammonia then the solution was kept aside for half an hour and washed with water and ethanol solution by centrifugation followed by drying the sample overnight at 50 °C. The resulting material xerogel modified DE with thiol functionalization was designated as DE-XSH, and the material was stored in a desiccator until further use.

2.3 Synthesis of AgNP decorated diatom silica (DE-XSH-Ag)

To decorate AgNPs on thiol functionalized DE (DE-XSH), the silver nanoparticles were synthesized *in situ* in the presence of DE-XSH. A 25 mL of 3.55mM sodium citrate solution was mixed with the 20 mL of 2 mM sodium borohydride and heated up to the 60°C. The pre-synthesized DE-XSH (250 mg) was mixed with 10 mL of 4 mM $AgNO_3$ solution. This solution was added to the above-preheated sodium citrate, and sodium borohydride solution after the addition solution changed to yellowish color from colorless. The solution was further heated for 15 min by increasing the temperature to 80 °C. After cooling down the reaction mixture at room temperature, the AgNP nanoparticle decorated DE-XSH sample was separated by centrifugation. Followed by washing with water to remove the free AgNP and other unreacted species from the reaction mixture and dried overnight at 50 °C. The resulting material was designated as DE-XS-Ag, that was stored in a desiccator until further use.

2.4 Synthesis of AuNP decorated diatom silica (DE-XSH-Au)

Similarly, as mentioned earlier, like for AgNP, to decorate AuNPs on thiol functionalized DE (DE-XSH), the AuNPs were synthesized *in-situ*, with DE-XSH present in a reaction

mixture with metal precursors. In brief, 250 mg of pre-synthesized DE-XSH powder was dispersed in with the 10 mL of 4 mM $HAuCl_4$ solution and boiled for ten minutes. Then 1 mL of 0.1552 mM trisodium citrate was added to the above solution and stirred continuously for one hour. After some time, the solution changed to light pink color from colorless then the solution was centrifuged to remove the free AuNPs from the reaction mixture and dried overnight at 50 °C. The resulting material was designated as DE-XSH-Au, that was stored in a desiccator until further use.

2.5 Catalytic oxidation of glucose

A 10 mg of the catalysts (DE-XS-Au/ DE-XS-Ag) was suspended in 5 mL of water and added to the 10 mL of 0.05 mol/L glucose solution into the three-necked flask and heated at 45 °C with continuous stirring at 550 rpm. Insert oxygen gas through bubbling in the solution with a 500 mL/min flow rate (one bubble per second). The pH of the reaction was maintained at 9 by using 0.1 N NaOH before starting the reaction and kept constant during the experiment. At the end of the reaction, D-glucose is converted into gluconic acid and the product was separated by the centrifugation method. The collected product was used for further characterization and to determine the amount of remaining D-glucose in reaction by titrating supernatant using Fehling's titration method(Fischer et al. 2016).

2.6 Catalytic dye degradation studies

Additionally, the catalytic activity of DE-XSH-Au and DE-XSH-Ag was tested for the degradation of various dyes like MB, and CY at room temperature, 28ºC. At a consistent time, interval, 2 mL of the mixture were taken out from the reaction mixture and filtrated using a 0.22 µm syringe filter to remove the catalyst particles altogether. The dye concentration in the solution was measured by UV-Visible spectrophotometer (ShimadzuUV-1800) at the maximum absorption wavelength of dye. The dye degradation efficiency was determined using the following equation.

Degradation efficiency (%) = $(C_0 - C)/C_0 \times 100\%$.

Where C_0 was the initial dye concentration and C was the dye at a specific concentration-time t during the reaction.

2.7 Characterization

All the materials DE, DE-XSH, DE-XSH-Au, and DE-XSH-Ag were characterized by various techniques to confirm the surface modification and incorporation of Nobel metal nanoparticles like AuNPs and AgNPs. A field emission scanning electron microscope (FESEM JEOL JSM 7100 F) was used to understand the surface morphological characteristics of DE, DE-XSH. The sample analysis was performed by drop-casting the sample on silicon wafers and drying it overnight. Also, the energy-dispersive X-ray spectroscopy (EDAX) was carried out for the same sample to know the chemical composition of the materials after incorporating AuNPs and AgNPs. The transmission electron microscope (TEM) Technai T-20 at an operating voltage of 200 kV was used to acquire high-resolution images. The samples were dispersed in ethanol and ultra-sonicated for 5 min. A small drop of the sample, 5 µl, was then taken in a carbon-coated copper grid and dried before viewing(Li et al. 2022; Singh et al. 2021). The Brunauer-Emmett-Teller (BET) surface area measurement was carried out to understand the textural properties of the materials, DE, DE-XSH, DE-XSH-Au, and DE-XSH-Ag using liquid N_2 at a temperature of -196 °C on a Belsorp-Max (M/s. Microtrac BEL, Japan). The samples were pre-heated at 100 °C for 2 h to expel the interlayer moisture under a vacuum before BET measurements. The AT-IR, attenuated total reflectance infrared spectra were recorded on Bruker Alpha Eco-ATR spectrometer in the range of 4000 – 500 cm^{-1}. For all the samples before, after surface modification, and after nanoparticle incorporation, the IR spectra were recorded. Powder X-ray diffraction patterns of DE, DE-XSH, DE-XSH-Au, and DE-XSH-Ag were recorded on an UltimaIV X-ray diffractometer (Rigaku Corporation, Japan) using Ni-filtered Cu Kα radiation (l = 1.5406 A°) with a 2θ scan speed of 1.0° min^{-1} and a 2θ scan range of 5–80° at 40 kV and 30mA. The magic-angle spinning (MAS) solid-state NMR study was carried out on a BRUKER NMR spectrometer, 400 MHz, under ambient conditions. The ^{29}Si NMR spectra were recorded at 99.37 MHz using a 4 mm rotor probe with TMS as an external standard. Thermogravimetric analysis (TGA) was carried out on Pekin Elmer Model STA 8000 instrument using N_2 as a purge gas.

3 Results and discussion

3.1 Characterization of materials: DE, DE-XSH, DE-XSH-Au, and DE-XSH-Ag

The FESEM images of bare DE (Aulacoseira sp) after purification process, post functionalization with thiol in DE-XSH, and after nanoparticle incorporation in DE-XSH-Au, and DE-XSH-Ag are depicted in Fig. 1. The SEM images of bare DE show porous structure with cylindrical frustules and no morphological alterations after the purification process (Fig. 1a, b). Significant alterations in the surface morphology were observed after xerogel modification and in situ functionalization with thiol in DE-XSH (Fig. 1c, d). Mostly the DE pores were moderately covered by xerogel

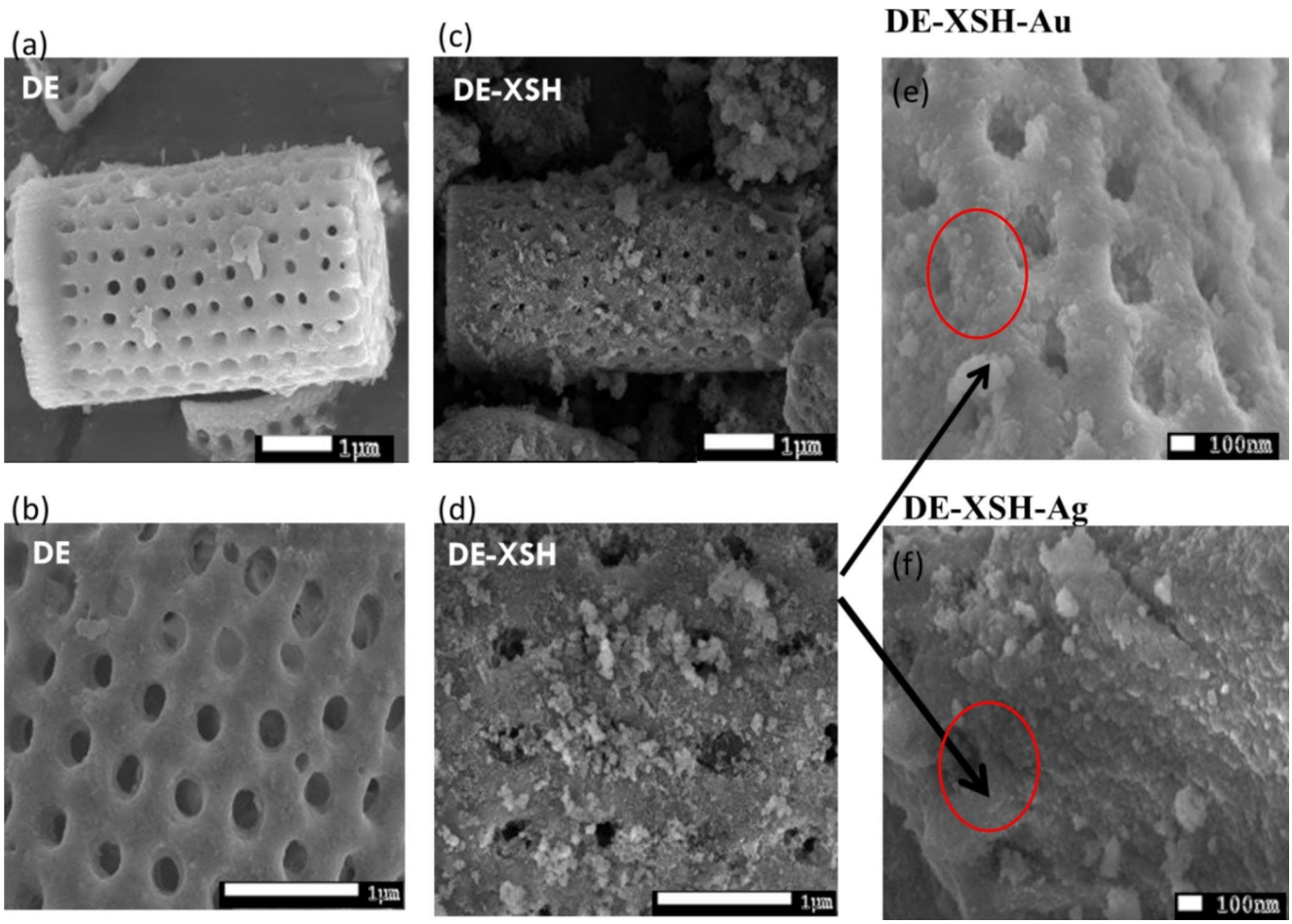

Fig. 1 FESEM images of (a, b) Diatom (DE); (c, d) DE-XSH, Post Functionalization with xerogel and thiol group; (e, f) high magnification image of DE-XSH-Au, and DE-XSH-Ag where the arrow indicates AuNP and AgNP consistently dispersed on modified DE surface

particles on the surface. In some cases, large particles of xerogel were anchored to DE. The empirical findings are in agreement with our previously reported work on surface-modified diatoms (Uthappa et al. 2018a). High magnification images of DE-XSH-Au and DE-XSH-Ag are shown in Fig. 1e, f., depicting the tethered xerogel particles on the DE surface and tiny nanoparticles (AuNP and AgNP) in DE-XSH-Au, and DE-XSH-Ag, respectively.

Additionally, EDAX analysis was also carried out to approve the presence of expected elements as shown in Fig. 2. It is well established that silica and oxygen are the main constituents present in DE. Subsequently, after surface functionalization in DE-XSH, it shows the presence of sulphur as expected along with "Si" and "O" [Fig. 2 A (c, d) and Fig. 2B (c, d)]. Conversely, the EDAX analysis was performed on nanoparticle incorporated samples i.e., DE-XSH-Au, and DE-XSH-Ag. The presence of Au and Ag elements and sulphur can be seen in Fig. 2 A (e) and 2B (e) respectively. The elemental composition of all the materials is shown in Table 1.

The N_2 adsorption-desorption isotherms of all the materials, DE, DE-XSH, DE-XSH-Ag, and DE-XSH-Au, are shown in Fig. 3. According to the IUPAC classification, a type of IV isotherm was observed for all the materials (Fig. 3a, b) that exhibited an H1 hysteresis loop characteristic of mesoporous materials classically silica(Brunauer et al. 1940; Hegde et al. 2022). The adsorption branch of each isotherm showed a sharp inflection indicating a typical capillary condensation within uniform pores, and also considerable adsorption amounts specify the considerable volume of nano spaces available even after the functionalization (Fig. 3c, d).

Furthermore, the BET surface area analysis was carried out to understand the textural properties of the materials; DE, DE-XSH, DE-XSH-Au, and DE-XSH-Ag(Singh et al. 2018). The observed results are shown in Table 2. The bare DE shows a very less surface area value, 18.0 m^2/g. After surface functionalization with MTPMS, the surface area increased to 500 m^2/g. The increase in the surface area on the diatom frustule is due to the presence of fine xerogel

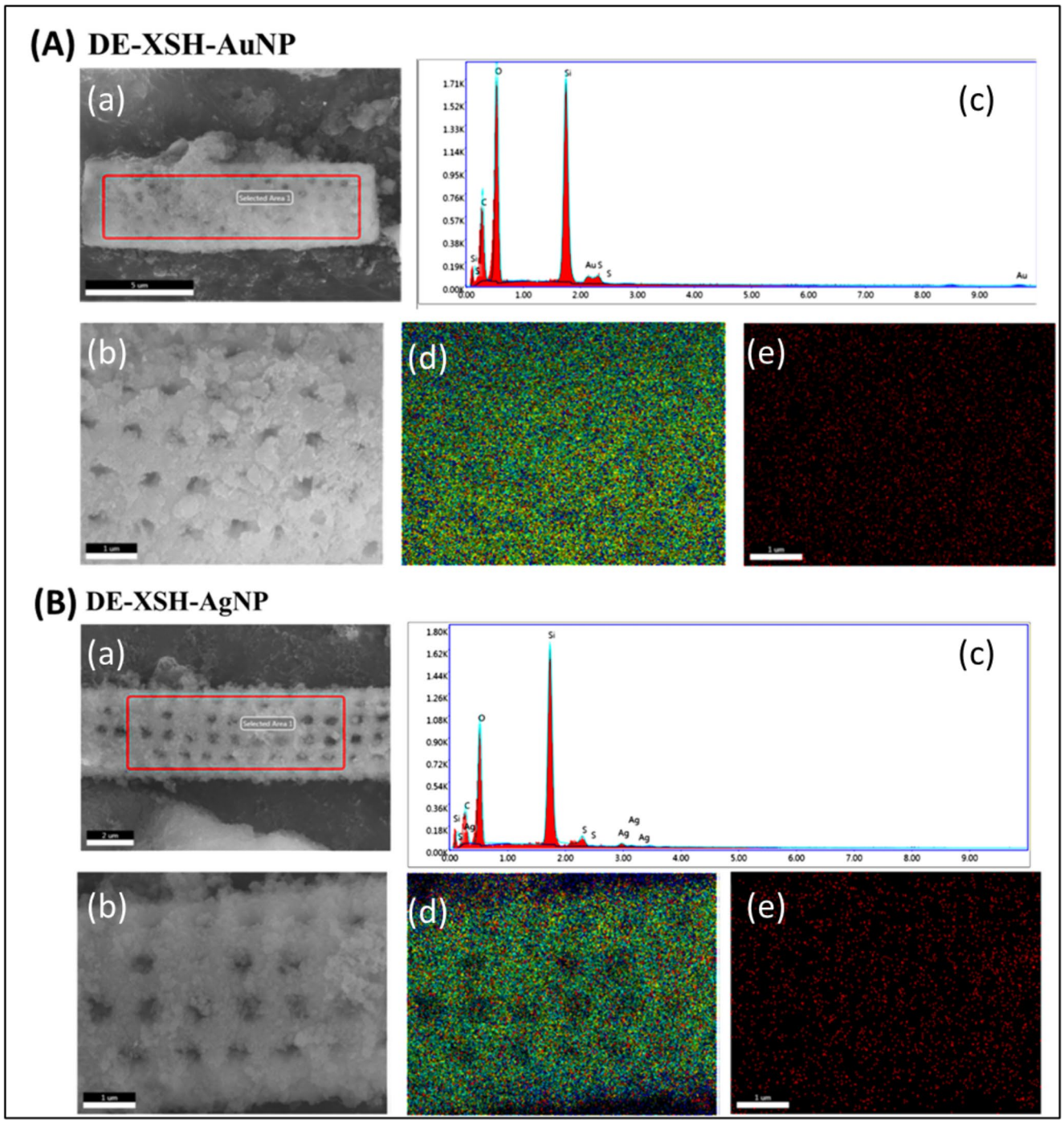

Fig. 2 (A) FESEM images of (a, b) DE-XSH-Au; (c, d, e) EDAX elemental mapping for DE-XSH-Au confirmed the presence of Si, O, S and Au. (B) FESEM images of (a, b) DE-XSH-Ag; (c, d, e) EDAX elemental mapping for DE-XSH-Ag confirmed the presence of Si, O, S and Ag

Table 1 % Element's present in DE, DE-XSH, DE-XSH-Au, and DE-XSH-Ag

Materials	% Elemental composition				
	Si	O	S	Au	Ag
DE	38	59	-	-	-
DE-XSH	36	57	2.20		
DE-XSH-Au	20.34	46	1.74	1.15	-
DE-XSH-Ag	30.12	40	2.14	-	1.93

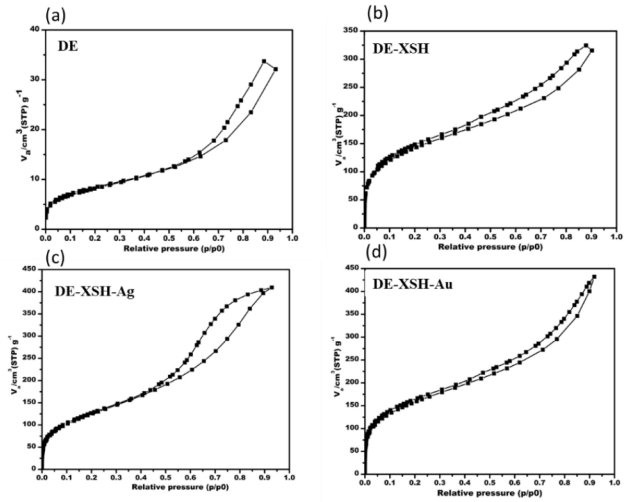

Fig. 3 N_2 adsorption-desorption isotherms of (a) DE, (b) DE-XSH, (c) DE-XSH-Ag (d) DE-XSH-Au

Table 2 Textural properties of materials

Sample	Surface area (m^2/g)	Pore diameter(nm)
DE	18	500
DE-XSH	501	4.42
DE-XSH-Ag	435	3.92
DE-XSH-Au	428	2.52

and functionalization. Post encapsulation of AuNPs and AgNPs in DE-XSH-Au and DE-XSH-Ag, respectively, the surface area decreases due to nanoparticles blocking pores, as shown in Table 2.

ATR-IR analysis was carried out to confirm the surface modification and organosilylation on the DE surface. As shown in Fig. 4 A, bare DE depicts a characteristics band at 1100 cm^{-1} that can be due to the asymmetric stretching of Si-O-Si. Another stretching vibration at 799 cm^{-1} is attributed to Al-O-Si. A stretching vibration of the zeolitic water source was observed at 1634 cm^{-1} from DE. Additionally, a broad peak in the range of 3100–3700 cm^{-1} corresponds to O-H stretching vibration due to physiosorbed water molecules being consistent in all the materials(Uthappa et al. 2018a). After surface functionalization on the DE surface, the weak band around 2550 to 2600 cm^{-1} was observed in DE-XSH, *DE-XSH-Au, and DE-XSH-Ag* which is attributed to -SH thiol groups. This confirms the -SH, thiol functionalization after organosilylation using MPTMS. The investigational findings are in good agreement with the reported one (Yan et al. 2019). ^{29}Si MAS NMR further investigated the functionalization of DE in imminent sections.

The powder X-ray diffraction (XRD) pattern shown in Fig. 4B revealed that DE exhibits peaks at the 2Θ range of 20° and 26° due to the inherently amorphous nature of diatom biosilica. The hexagonal structure of the quartz crystalline peak is present at 21.5° and 26.7°, accredited to the (100) and (011) planes respectively match well with JCPDS file no. 89–8934 [28] as shown in Fig. 4B. Post functionalization in DE-XSH, the amorphous nature of bare DE is retained. Post decoration with nanoparticles in DE-XSH-Au and DE-XSH-Ag, the presence of additional diffraction peaks corresponding to respective gold and silver nanoparticles confirms their occurrence. Specifically in DE-XSH-Ag, four diffraction peaks at 38.1°, 44.3°, 64.5°, and 77.4° were observed in 2Θ range that corresponds to the (111), (200), (220), and (311) planes [40] which match well with Joint Committee on Powder Diffraction Standards (JCPDS file no.39–1451) signifying the presence of AgNPs (Han et al. 2012) as shown in Fig. 4B. Whereas in the case

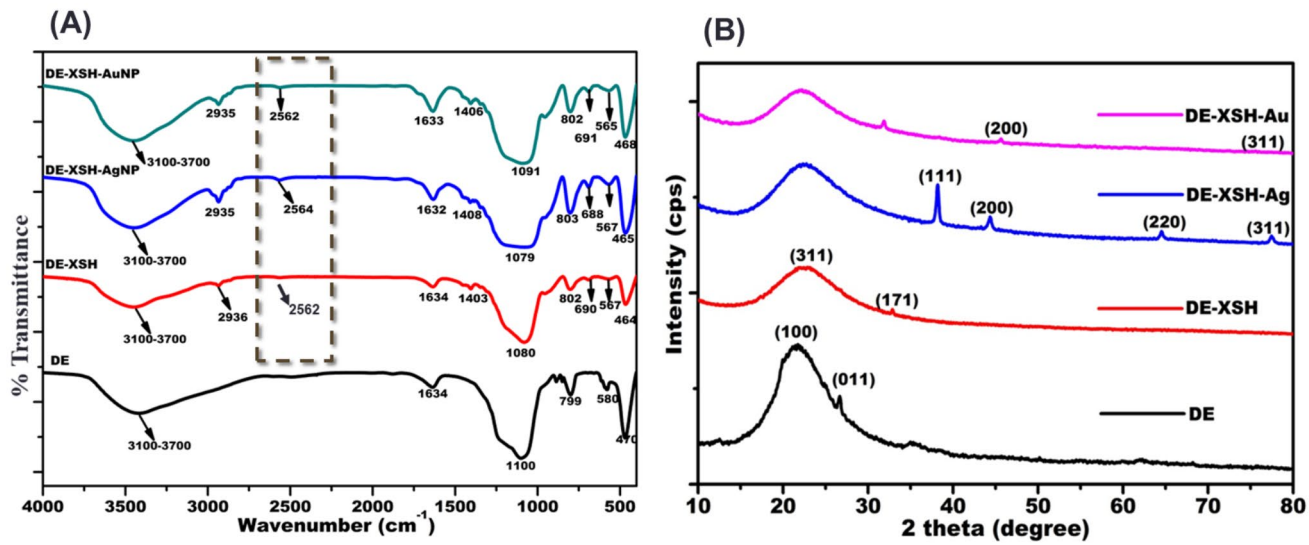

Fig. 4 (A) ATIR spectra of; DE, DE-XSH, DE-XSH-Au, and DE-XSH-Ag (B) XRD patterns for; DE, DE-XSH, DE-XSH-Au, and DE-XSH-Ag

of DE-XSH-Au, there were four well defined characteristic peaks at 38.6°, 45.6°, 65.12°, and 78.11° respectively indexed to (111), (200), (220), and (311) reflections of metallic gold. The interplanar spacing values and the lattice parameters were matched well with JCPDS, gold file No. 04-0784.

The materials were further analysed by TEM to get more insights into the dispersion of AgNPs and AuNPs on functionalized diatoms in DE-XSH-Au and DE-XSH-Ag (Fig. 5). The fine decoration of well-dispersed gold nanoparticles without aggregation was observed in DE-XSH-Au, as shown in Fig. 5 (a, b). The nanoparticles are virtually spherical in shape and measure around 30 nm, as shown in Fig. 5 (a, b). Whereas in the case of DE-XSH-Ag, the aggregated silver nanoparticles can be observed on the surface of functionalized diatom silica (Fig. 5c, d). In the present case, gold and silver nanoparticles are synthesized by in situ method over thiol functionalized diatoms. The size distribution of AuNP and AgNP on DE surface was studied from TEM images. The well distributed AuNP and AgNP were observed from TEM images. The average size for AuNP and AgNP nanoparticles was 101 and 31 nm respectively as shown in figure S1.

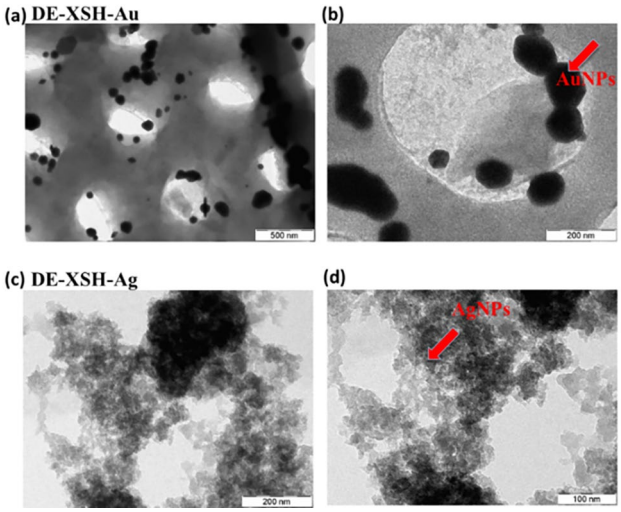

Fig. 5 TEM images of (a, b) DE-XSH-Au, and (c, d) DE-XSH-Ag where AuNP and AgNP are consistently dispersed on a modified DE-XSH surface. The arrow indicates the nanoparticles on DE surface

The ^{29}Si MAS NMR spectra are shown in Fig. 6. The bare DE exhibited the qualitative pattern of Q units typical of amorphous silica (Fig. 6a) as obtained from CP MAS NMR and was comparable to that reported for different diatom species earlier(Lang et al. 2013). The surface-functionalized diatoms, DE-XSH, exhibited mainly two chemical shifts, as shown in Fig. 6b. The T units (T2 and T3 at -58.7 and − 64.1 ppm respectively) and Q units (Q2, Q3, and Q4 at -93.0, -101.5, and − 110.4 pm, respectively). In comparison with bare DE, the presence of T2 and T3 units in MPTMS-modified diatoms, DE-XSH, confirmed the presence of an organic moiety with -SH group pending from the Si backbone of the hybrid skeleton of diatoms. This aspect was further confirmed by the pattern of Q units obtained from the ^{29}Si-MAS NMR functionalized diatoms (DE-XSH, DE-XSH-Au, DE-XSH-Ag), with an increase in

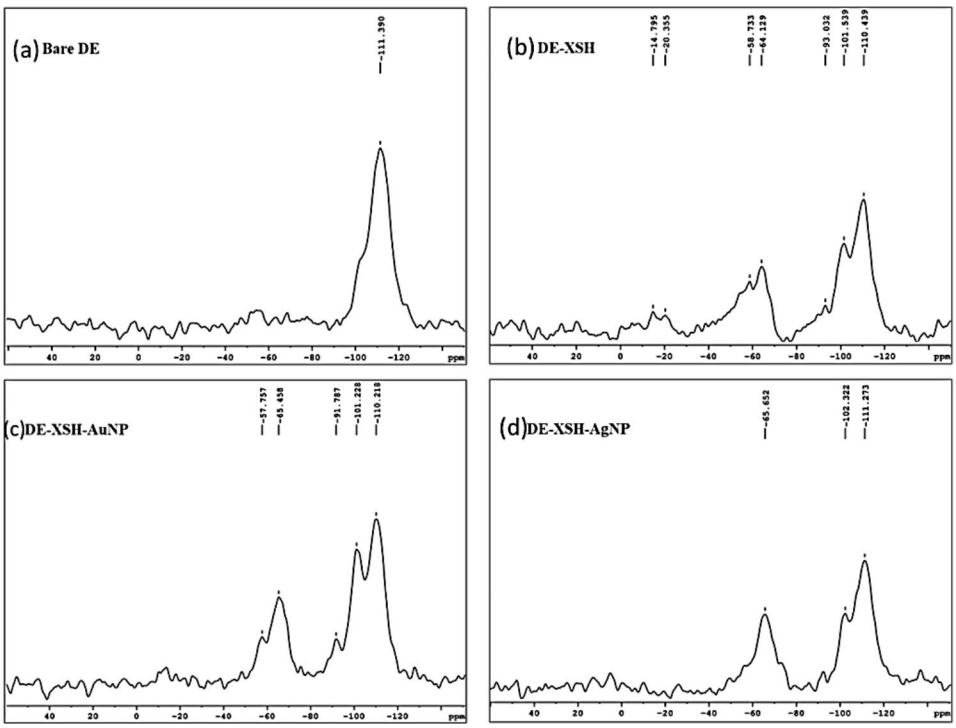

Fig. 6 ^{29}Si-MAS NMR spectra of bare DE and functionalized diatoms DE-XSH, DE-XSH-Au, DE-XSH-Ag

the intensity ratio between Q3 and Q4 units (Fig. 6c, d). The experimental findings are in agreement with the previous reports (Wisser et al. 2015).

The TGA–DTA curves of bare DE, functionalized DE-XSH, and nanoparticle decorated DE-XSH-Au and DE-XSH-Ag are shown in Fig. 7. The bare DE (Fig. 7a) shows a weight loss of 7% at 50 °C to 130°C due to surface adsorbed water. 8% weight loss corresponding to the -SH group was observed at 150°C to 350°C in functionalized DE-XSH (Fig. 7b). All the materials were stable up to 550°C as observed in TGA curves, as shown in Fig. 7. After nanoparticle functionalization, the catalysts DE-SXH-Au and DE-XSH-Ag were found to be more stable as compared to DE-XSH and DE itself.

3.2 Oxidation of D-Glucose

The catalytic oxidation of D-glucose is reported by nanoparticles of different sizes (Franz et al. 2021; Sulman et al. 2007). In the current study, the nanoparticle decorated DE-XSH-Au and DE-XSH-Ag were investigated for oxidation of glucose by varying different parameters like nanoparticle loading, amount of catalyst, reaction time, and reaction temperature.

The control experiments were first conducted to check the activity of the original constituents of the catalysts, that is, only DE and DE-XSH. It is evident from Fig. 8 A that the DE and DE-XSH as such show the shallow conversion for glucose oxidation, whereas both the catalysts exhibit much higher conversion. The higher conversion of DE-XSH-Au and DE-XSH-Ag can be attributed to the presence of silver and gold nanoparticles as active sites and their high surface area (Table 2) as compared to bare DE. The DE exhibits surface area as low as 18 m^2 g^{-1}, whereas the catalyst *DE-XSH-Au and DE-XSH-Ag* exhibit much better conversion. The large surface area of catalysts, as shown in Table 2, enhances the accessibility of active catalytic sites in the present case of gold nanoparticles and silver nanoparticles

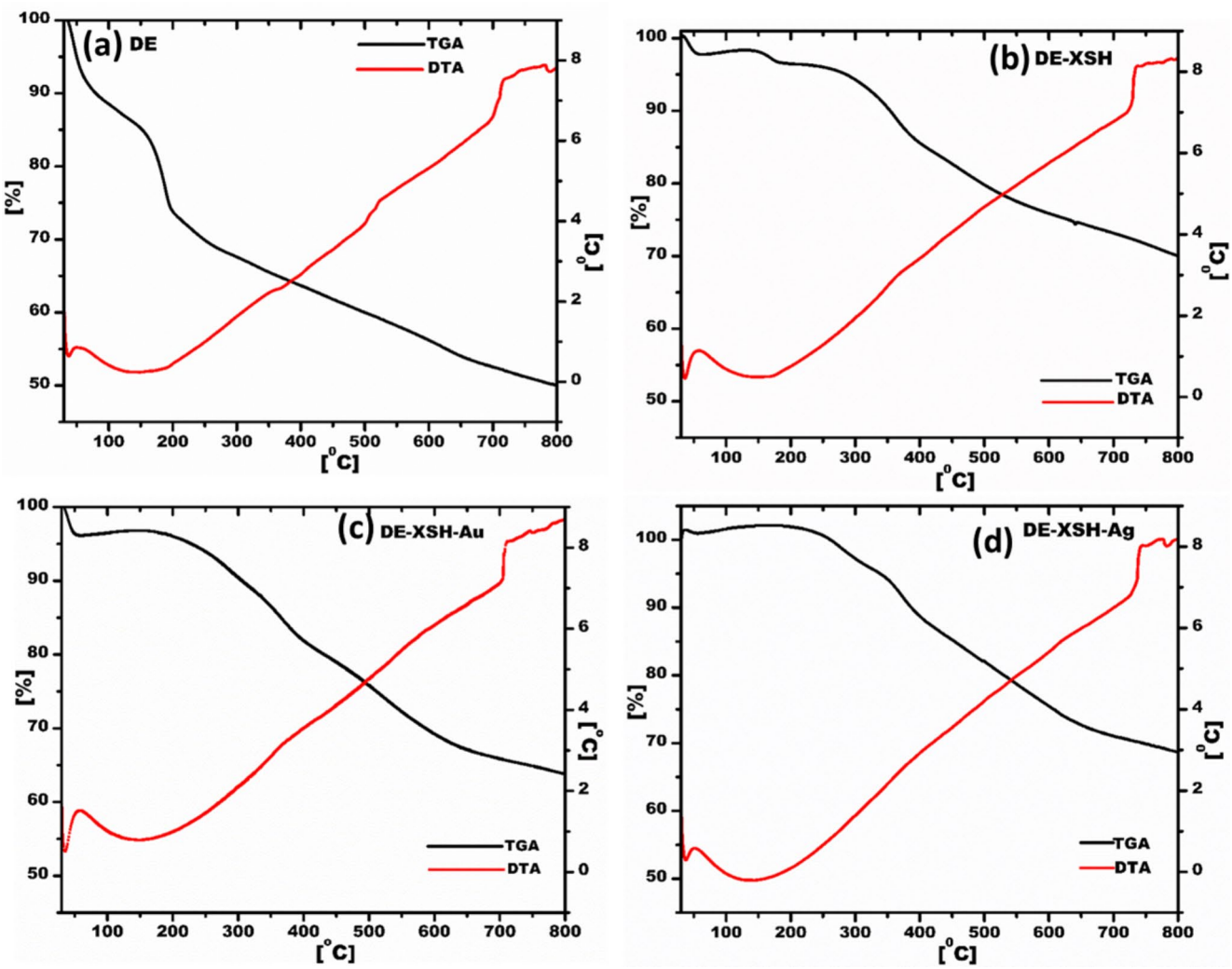

Fig. 7 TGA and DTA analysis of (a) DE (b) DE-XSH (c) DE-XSH-Au (d) DE-XSH-Ag

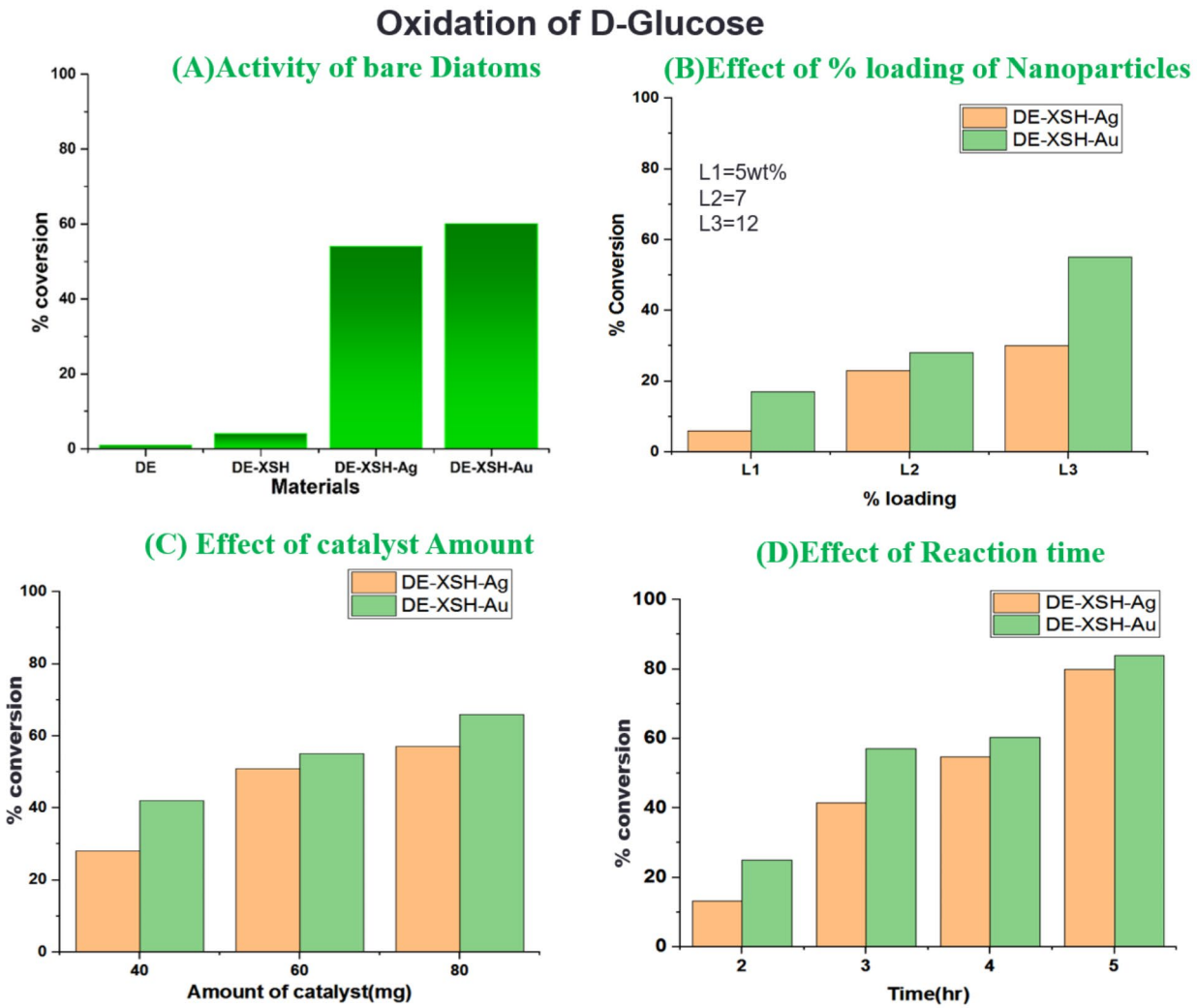

Fig. 8 (A) Control experiment, the activity of bare diatoms; Reaction conditions: the amount of catalyst 0.1 g, reaction temperature 45°C, reaction time 4 h. (B) Effect of % loading of catalyst (C) Effect of amount of catalyst; Reaction conditions: reaction temperature 45°C, reaction time 4 h (D) Effect of reaction time

in DE-XSH-Au and DE-XSH-Ag, respectively, which eventually explains the better activity. The high surface area and large pore diameter of the catalyst enable the more significant adsorption of the reactant molecules onto the catalyst and accessibility to active sites and eventually desorption of products. This explains the better performance of DE-XSH-Au and DE-XSH-Ag as compared to bare DE and functionalized DE-SXH in glucose oxidation. With the increase in nanoparticle loading from 5 to 12%, the glucose conversion increases, as shown in Fig. 8B.

The effect of the amount of catalyst on glucose conversion was investigated for both the catalysts. The amount of catalyst was varied in the range of 20-100 mg. As shown in Fig. 8 C, the conversion increased with the increase in the amount of catalysts (*DE-XSH-Au, and DE-XSH-Ag*) and reached a maximum conversion with 80 mg of catalyst. But with a further increase in the amount of catalyst, the glucose conversion remains constant. Hence, 80 mg of catalyst amount was optimized. The catalyst with silver nanoparticles *DE-XSH-Ag* exhibited 60% conversion, and the catalyst with gold nanoparticles showed 70% conversion of glucose. The effect of reaction time on the conversion of glucose was investigated, as shown in Fig. 8. It was observed from Fig. 8D that the glucose conversion increases with an increase in reaction time for both the catalysts. In five hours, the glucose conversion was 78% over DE-XSH-Ag and 87% over DE-XSH-Au, respectively. The optimized conditions for glucose oxidation are: the amount of catalyst 80 mg; Reaction Temperature of 80°C, and Reaction Time of 5 h over *DE-XSH-Ag* and *DE-XSH-Au*.

Furthermore, the potentials of *DE-XSH-Ag* and *DE-XSH-Au* catalysts in dye degradation of organic dyes

methylene blue (MB) and chrysoidine Y (CY) dye were explored as shown in Fig. 9. As a preliminary studies effect of the amount of catalyst on dye degradation efficacy was explored. With increases in the amount of catalyst, dye degradation efficiency increases as expected (Fig. 9 A). The maximum dye degradation for MB was 95% over DE-XSH-Au and 88% over DE-XSH-Ag. Whereas for CY, the dye degradation efficiency was 92% over DE-XSH-Au and 80% over DE-XSH-Ag (Fig. 9 A, B). Compared to the DE-XSH-Ag catalyst, DE-XSH-Au exhibited better performance in glucose oxidation and dye degradation efficiency, which can be attributed to the inherent characteristics of gold nanoparticles.

3.3 Mechanism of oxidation of D-Glucose and dye degradationThe adsorption of reactants in present case D-Glucose or dyes, on catalyst surface enables activation and diffusion of reactants to active sites where actual chemical reaction occurs via formation of intermediates. The efficient synergistic effect of adsorption and oxidation catalysis by DE-XSH-Au and DE-XSH-Ag results in efficient conversion in D-Glucose oxidation and dye degradation. The role of adsorption in

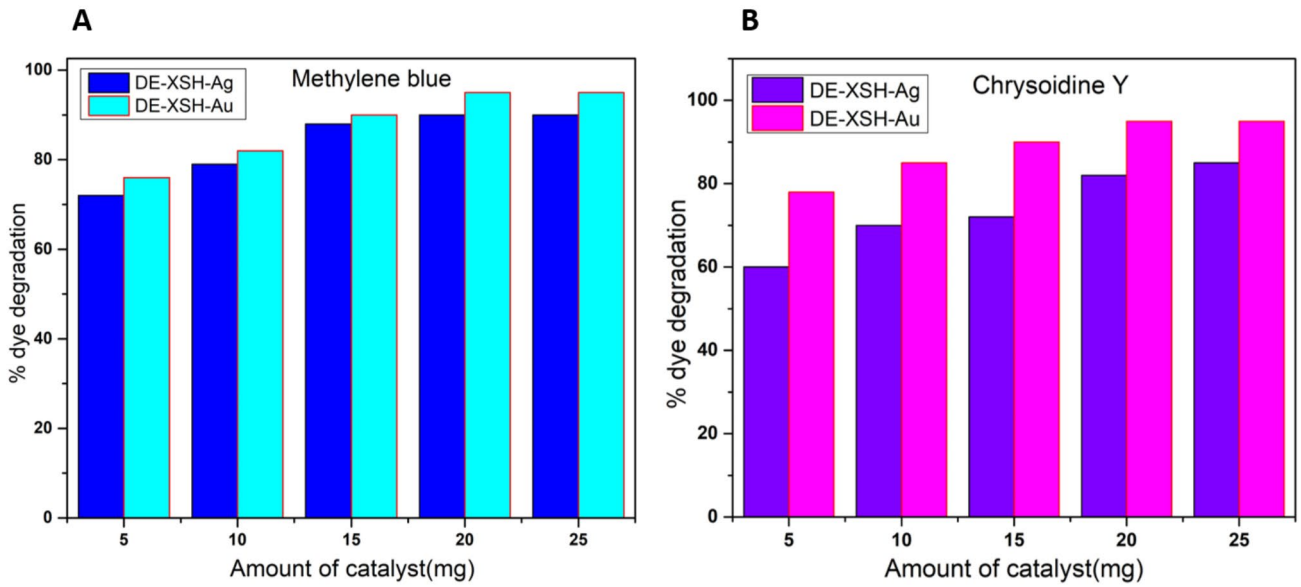

Fig. 9 (A) Effect of catalyst amount on the degradation of MB (B) effect of the amount of catalyst on the degradation of CY. The amount of catalyst was varied from 5 to 25 mg; dye concentration, 100 ppm; reaction time, 60 min

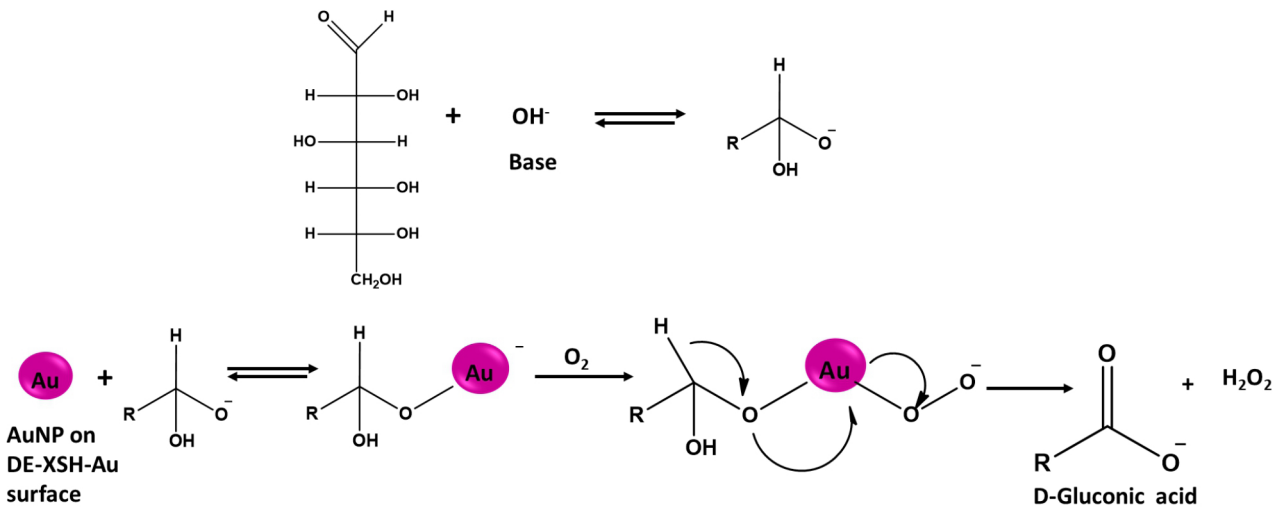

Scheme 3 Proposed Mechanism of oxidation of D- Glucose to D-Gluconic acid using molecular oxygen over DE-XSH-Au

heterogonous catalysis for various applications is well documented in literature (Chen et al., 2021).

The proposed mechanism of glucose oxidation in presence of molecular oxygen over DE-XSH-Au catalyst is shown in Scheme 3. The glucose is converted to gluconic acid in presence of alkali as promoter and there is formation of hydrogen peroxide as by product. First the glucose is adsorbed on catalyst surface where the hydrated glucose anion binds with AuNP surface atoms resulting in an electron rich species. The molecular oxygen is activated by nucleophilic attack of this species. The main reactive oxygen species like peroxide have already been proposed as a reaction intermediate during oxidation of glucose(Comotti et al., 2006).

The proposed oxidative degradation mechanism for multiple dyes MB and CY over DE-XSH-Au and DE-XSH-Ag is as follows. The surface charge on catalyst is expected to be negative charge. Both MB and CV are positively charged dyes. Initially both the dyes are adsorbed on catalyst surface due electrostatic attraction and additionally by hydrogen bonding due to the presence of surface hydroxyl groups on catalyst surface. Post adsorption of dye molecules on the catalyst surface, follows the catalytic degradation of dye molecules into smaller fragments due to oxidation by active Au/Ag atoms on catalyst surface. As the degradation of MB is well studied in the literature, post dye degradation products from catalyst surface were isolated using extraction in ethyl acetate. The extracted MB degradation products were analyzed by GC-MS. The oxidation of MB is initiated by demethylation. Further the degradation products like monodemethylation, di-demethylation, tri-demethylation were formed. The complete demethylation of nitrogen is followed by ring opening and the observed mass fragments are shown in figure S2. The observed findings are in agreement with similar reported previously(He et al. 2018; Pithadia et al. 2021; Rauf et al. 2010).

4 Conclusions

In summary, surface-functionalized and nanoparticle decorated biosilica catalysts, DE-XSH-Au and DE-XSH-Ag were developed. FT-IR and ^{29}Si MAS NMR spectra confirm the -SH, thiol functionalization after organosilylation in DE-XSH. XRD, SEM, and TEM show that the DE surface is uniformly decorated with nanoparticles in DE-XSH-Au and DE-XSH-Ag without disturbing the unique morphology of diatom frustules. The present catalysts DE-XSH-Au and DE-XSH-Ag exhibit excellent activity in the oxidation of glucose under mild conditions. Also, the catalyst shows the potential of being used as an excellent material for dye degradation of methylene blue, and chrysoidine Y. This rapid and excellent catalytic activity of DE-XSH-Au and DE-XSH-Ag catalyst is attributed to the highly porous morphology of the modified diatom biosilica, which acts as the matrix for AuNP and AgNP. The high surface area and porous morphology enhances the reaction extent, demonstrating a highly efficient catalytic activity in oxidation and dye degradation. These results suggest an opportunity for these materials in water remediation applications.

Supplementary information The online version contains supplementary material available at https://doi.org/10.1007/s10934-022-01262-w.

Acknowledgements We are thankful to Jain University, Bangalore, India, for providing facilities.

Authors' contributions: Authors' contributions: Conceptualization: Varsha Brahmkhatri, Mahaveer D. Kurkuri, Methodology: Parimal Pandit, Pranita Rananaware, Aviva D'Souza, Formal analysis, and investigation: Parimal Pandit, Pranita Rananaware Writing - original draft preparation: Parimal Pandit and Pranita Rananaware, Writing – review, and editing: Varsha Brahmkhatri, Mahaveer D. Kurkuri, Supervision: Varsha Brahmkhatri, Mahaveer D. Kurkuri,

Funding: We acknowledge TARE-SERB File NO: TAR/2018/000547 for funding.

Availability of data and material: All data and material regarding this work are completely transparent.

Code Availability Not applicable.

Declarations

Conflict of interest There are no conflicts of interest to declare.

References

M.R. Abukhadra, M.A. Sayed, A.M. Rabie, S.A. Ahmed, Surface decoration of diatomite by Ni/NiO nanoparticles as hybrid composite of enhanced adsorption properties for malachite green dye and hexavalent chromium. Colloids Surf., A **577**, 583–593 (2019). doi:https://doi.org/10.1016/j.colsurfa.2019.06.018

Z.H. Aitken, S. Luo, S.N. Reynolds, C. Thaulow, J.R. Greer, 2016. Microstructure provides insights into evolutionary design and resilience of Coscinodiscus sp. frustule. Proceedings of the National Academy of Sciences 113, 2017–2022, doi:https://doi.org/10.1073/pnas.1519790113

G. Bayramoglu, A. Akbulut, M. Yakup Arica, Immobilization of tyrosinase on modified diatom biosilica: Enzymatic removal of phenolic compounds from aqueous solution. J. Hazard. Mater. **244–245**, 528–536 (2013). doi:https://doi.org/10.1016/j.jhazmat.2012.10.041

V. Brahmkhatri, P. Pandit, P. Rananaware, A. D'Souza, M.D. Kurkuri, Recent progress in detection of chemical and biological toxins in Water using plasmonic nanosensors. Trends in Environmental

Analytical Chemistry **30**, e00117 (2021). doi:https://doi.org/10.1016/j.teac.2021.e00117
S. Briceño, E.A. Chavez-Chico, G. González, Diatoms decorated with gold nanoparticles by In-situ and Ex-situ methods for in vitro gentamicin release. Mater. Sci. Engineering: C **123**, 112018 (2021). doi:https://doi.org/10.1016/j.msec.2021.112018
S. Brunauer, L.S. Deming, W.E. Deming, E. Teller, On a Theory of the van der Waals Adsorption of Gases. J. Am. Chem. Soc. **62**, 1723–1732 (1940). doi:https://doi.org/10.1021/ja01864a025
T. Chen, Z. Zhu, H. Zhang, Y. Qiu, D. Yin, Cu-O-incorporation design for promoted heterogeneous catalysis: synergistic effect of surface adsorption and catalysis towards efficient bisphenol A removal. Appl. Surf. Sci. **569**, 151107 (2021). doi:https://doi.org/10.1016/j.apsusc.2021.151107
L. Chetia, D. Kalita, G.A. Ahmed, Synthesis of Ag nanoparticles using diatom cells for ammonia sensing. Sens. Bio-Sensing Res. **16**, 55–61 (2017). doi:https://doi.org/10.1016/j.sbsr.2017.11.004
M. Comotti, C. Della Pina, E. Falletta, M. Rossi, Aerobic Oxidation of Glucose with Gold Catalyst: Hydrogen Peroxide as Intermediate and Reagent. Adv. Synth. Catal. **348**, 313–316 (2006). doi:https://doi.org/10.1002/adsc.200505389
L. De Stefano, A. Lamberti, L. Rotiroti, M. De Stefano, Interfacing the nanostructured biosilica microshells of the marine diatom Coscinodiscus wailesii with biological matter. Acta Biomater. **4**, 126–130 (2008). doi:https://doi.org/10.1016/j.actbio.2007.09.003
J. Delasoie, F. Zobi, Natural Diatom Biosilica as Microshuttles in Drug Delivery Systems. Pharmaceutics **11**, 537 (2019)
G. Della Rosa, D. Vona, A. Aloisi, R. Ragni, R. Di Corato, M. Lo Presti, S.R. Cicco, E. Altamura, A. Taurino, M. Catalano, G.M. Farinola, R. Rinaldi, Luminescent Silica-Based Nanostructures from in Vivo Iridium-Doped Diatoms Microalgae. ACS Sustain. Chem. Eng. **7**, 2207–2215 (2019). doi:https://doi.org/10.1021/acssuschemeng.8b04888
J.E.N. Dolatabadi, M. de la Guardia, Applications of diatoms and silica nanotechnology in biosensing, drug and gene delivery, and formation of complex metal nanostructures. TRAC Trends Anal. Chem. **30**, 1538–1548 (2011). doi:https://doi.org/10.1016/j.trac.2011.04.015
J. Esfandyari, B. Shojaedin-Givi, H. Hashemzadeh, M. Mozafari-Nia, Z. Vaezi, H. Naderi-Manesh, Capture and detection of rare cancer cells in blood by intrinsic fluorescence of a novel functionalized diatom. Photodiagn. Photodyn. Ther. **30**, 101753 (2020). doi:https://doi.org/10.1016/j.pdpdt.2020.101753
C. Feng, J. Li, G.S. Wu, Y.Z. Mu, M. Kong, C.Q. Jiang, X.J. Cheng, Y. Liu, X.G. Chen, Chitosan-Coated Diatom Silica as Hemostatic Agent for Hemorrhage Control. ACS Appl. Mater. Interfaces **8**, 34234–34243 (2016). doi:https://doi.org/10.1021/acsami.6b12317
C. Fischer, M. Adam, A.C. Mueller, E. Sperling, M. Wustmann, K.-H. van Pée, S. Kaskel, E. Brunner, Gold Nanoparticle-Decorated Diatom Biosilica: A Favorable Catalyst for the Oxidation of d-Glucose. ACS Omega **1**, 1253–1261 (2016). doi:https://doi.org/10.1021/acsomega.6b00406
S. Franz, N.D. Shcherban, I. Bezverkhyy, S.A. Sergiienko, I.L. Simakova, T. Salmi, D.Y. Murzin, Catalytic activity of gold nanoparticles deposited on N-doped carbon-based supports in oxidation of glucose and arabinose mixtures. Res. Chem. Intermed. **47**, 2573–2587 (2021). doi:https://doi.org/10.1007/s11164-021-04426-6
P. Gholami, A. Khataee, A. Bhatnagar, Environmentally superior cleaning of diatom frustules using sono-Fenton process: Facile fabrication of nanoporous silica with homogeneous morphology and controlled size. Ultrason. Sonochem. **64**, 105044 (2020). doi:https://doi.org/10.1016/j.ultsonch.2020.105044
S. Gupta, M. Kashyap, V. Kumar, P. Jain, V. Vinayak, K.B. Joshi, Peptide mediated facile fabrication of silver nanoparticles over living diatom surface and its application. J. Mol. Liq. **249**, 600–608 (2018). doi:https://doi.org/10.1016/j.molliq.2017.11.086
J.J. Gutiérrez Moreno, K. Pan, Y. Wang, W. Li, Computational Study of APTES Surface Functionalization of Diatom-like Amorphous SiO2 Surfaces for Heavy Metal Adsorption. Langmuir **36**, 5680–5689 (2020). doi:https://doi.org/10.1021/acs.langmuir.9b03755
J. Han, P. Fang, W. Jiang, L. Li, R. Guo, Ag-Nanoparticle-Loaded Mesoporous Silica: Spontaneous Formation of Ag Nanoparticles and Mesoporous Silica SBA-15 by a One-Pot Strategy and Their Catalytic Applications. Langmuir **28**, 4768–4775 (2012). doi:https://doi.org/10.1021/la204503b
Y. He, D.B. Jiang, J. Chen, D.Y. Jiang, Y.X. Zhang, Synthesis of MnO2 nanosheets on montmorillonite for oxidative degradation and adsorption of methylene blue. J. Colloid Interface Sci. **510**, 207–220 (2018). doi:https://doi.org/10.1016/j.jcis.2017.09.066
V. Hegde, P. Pandit, P. Rananaware, V.P. Brahmkhatri, Sulfonic acid-functionalized mesoporous silica catalyst with different morphology for biodiesel production. Front. Chem. Sci. Eng. (2022). doi:https://doi.org/10.1007/s11705-021-2133-z
A. Jantschke, A.K. Herrmann, V. Lesnyak, A. Eychmüller, E. Brunner, Decoration of diatom biosilica with noble metal and semiconductor nanoparticles (< 10 nm): assembly, characterization, and applications. Chem. Asian J. **7**, 85–90 (2012). doi:https://doi.org/10.1002/asia.201100563
A. Kamińska, M. Sprynskyy, K. Winkler, T. Szymborski, Ultrasensitive SERS immunoassay based on diatom biosilica for detection of interleukins in blood plasma. Anal. Bioanal. Chem. **409**, 6337–6347 (2017). doi:https://doi.org/10.1007/s00216-017-0566-5
S. Kim, K.I. Joo, B.H. Jo, H.J. Cha, Stability-Controllable Self-Immobilization of Carbonic Anhydrase Fused with a Silica-Binding Tag onto Diatom Biosilica for Enzymatic CO2 Capture and Utilization. ACS Appl. Mater. Interfaces **12**, 27055–27063 (2020). doi:https://doi.org/10.1021/acsami.0c03804
A.M. Korsunsky, Y.D. Bedoshvili, J. Cvjetinovic, P. Aggrey, K.I. Dragnevski, D.A. Gorin, A.I. Salimon, Y.V. Likhoshway, 2020. Siliceous diatom frustules – A smart nanotechnology platform. Materials Today: Proceedings 33, 2032–2040, doi:https://doi.org/10.1016/j.matpr.2020.08.571
F. Kucuk, S. Sismanoglu, Y. Kanbur, U. Tayfun, Effect of silane-modification of diatomite on its composites with thermoplastic polyurethane. Mater. Chem. Phys. **256**, 123683 (2020). doi:https://doi.org/10.1016/j.matchemphys.2020.123683
Y. Lang, F. del Monte, L. Collins, B.J. Rodriguez, K. Thompson, P. Dockery, D.P. Finn, A. Pandit, Functionalization of the living diatom Thalassiosira weissflogii with thiol moieties. Nat. Commun. **4**, 3683 (2013). doi:https://doi.org/10.1038/ncomms3683
S. Leonardo, B. Prieto-Simón, M. Campàs, Past, present and future of diatoms in biosensing. TRAC Trends Anal. Chem. **79**, 276–285 (2016). doi:https://doi.org/10.1016/j.trac.2015.11.022
W. Li, G. Hua, J. Cai, Y. Zhou, X. Zhou, M. Wang, X. Wang, B. Fu, L. Ren, 2022. Multi-Stimulus Responsive Multilayer Coating for Treatment of Device-Associated Infections. J. Funct. biomaterials 13, 24, doi:https://doi.org/10.3390/jfb13010024
D. Liu, J. Gu, Q. Liu, Y. Tan, Z. Li, W. Zhang, Y. Su, W. Li, A. Cui, C. Gu, D. Zhang, Metal-organic frameworks reactivate deceased diatoms to be efficient CO(2) absorbents. Adv. Mater. **26**, 1229–1234 (2014). doi:https://doi.org/10.1002/adma.201304284
Y. Maeda, Y. Niwa, H. Tang, D. Kisailus, T. Yoshino, T. Tanaka, Development of Titania-Integrated Silica Cell Walls of the Titanium-Resistant Diatom, Fistulifera solaris. ACS Appl. Bio Mater. **1**, 2021–2029 (2018). doi:https://doi.org/10.1021/acsabm.8b00520
M. Mishra, A.P. Arukha, T. Bashir, D. Yadav, G.B.K.S. Prasad, 2017. All New Faces of Diatoms: Potential Source of Nanomaterials and Beyond. Front. Microbiol. 8, doi:https://doi.org/10.3389/fmicb.2017.01239

M.D. Moreno, K. Ma, J. Schoenung, L.P. Dávila, An integrated approach for probing the structure and mechanical properties of diatoms: Toward engineered nanotemplates. Acta Biomater. **25**, 313–324 (2015). doi:https://doi.org/10.1016/j.actbio.2015.07.028

V. Onesto, M. Villani, M.L. Coluccio, R. Majewska, A. Alabastri, E. Battista, A. Schirato, D. Calestani, N. Coppedé, M. Cesarelli, F. Amato, E. Di Fabrizio, F. Gentile, Silica diatom shells tailored with Au nanoparticles enable sensitive analysis of molecules for biological, safety and environment applications. Nanoscale Res. Lett. **13**, 94–94 (2018). doi:https://doi.org/10.1186/s11671-018-2507-4

V. Panwar, T. Dutta, Diatom Biogenic Silica as a Felicitous Platform for Biochemical Engineering: Expanding Frontiers. ACS Appl. Bio Mater. **2**, 2295–2316 (2019). doi:https://doi.org/10.1021/acsabm.9b00050

D. Pithadia, V. Hegde, V.P. Brahmkhatri, A. Patel, New catalyst comprising Silicotungstic acid and MCM-22 for degradation of some organic dyes. Environ. Sci. Pollut. Res. **28**, 10633–10641 (2021). doi:https://doi.org/10.1007/s11356-020-11340-8

A. Prins, P. Deleris, C. Hubas, B. Jesus, 2020. Effect of Light Intensity and Light Quality on Diatom Behavioral and Physiological Photoprotection. Front. Mar. Sci. 7, doi:https://doi.org/10.3389/fmars.2020.00203

N. Rabiee, M. Khatami, J. Soufi, G. Fatahi, Y. Iravani, S. Varma, R. S, Diatoms with Invaluable Applications in Nanotechnology, Biotechnology, and Biomedicine: Recent Advances. ACS Biomaterials Science & Engineering **7**, 3053–3068 (2021). doi:https://doi.org/10.1021/acsbiomaterials.1c00475

M.A. Rauf, M.A. Meetani, A. Khaleel, A. Ahmed, Photocatalytic degradation of Methylene Blue using a mixed catalyst and product analysis by LC/MS. Chem. Eng. J. **157**, 373–378 (2010). doi:https://doi.org/10.1016/j.cej.2009.11.017

O. Şan, R. Gören, C. Özgür, Purification of diatomite powder by acid leaching for use in fabrication of porous ceramics. Int. J. Miner. Process. **93**, 6–10 (2009). doi:https://doi.org/10.1016/j.minpro.2009.04.007

A. Saxena, P. Kumar Singh, A. Bhatnagar, A. Tiwari, Growth of marine diatoms on aquaculture wastewater supplemented with nanosilica. Bioresour. Technol. **344**, 126210 (2022). doi:https://doi.org/10.1016/j.biortech.2021.126210

A. Shelar, A.V. Singh, R.S. Maharjan, P. Laux, A. Luch, D. Gemmati, V. Tisato, S.P. Singh, M.F. Santilli, A. Shelar, M. Chaskar, R. Patil, 2021. Sustainable Agriculture through Multidisciplinary Seed Nanopriming: Prospects of Opportunities and Challenges. Cells 10, doi:https://doi.org/10.3390/cells10092428

M.A. Sherief, G.T. El-Bassyouni, A.A. Gamal, M.A. Esawy, 2021. Modification of diatom using silver nanoparticle to improve antimicrobial activity. Materials Today: Proceedings 43, 3369–3374, doi:https://doi.org/10.1016/j.matpr.2020.05.391

A.V. Singh, T. Jahnke, V. Kishore, B.W. Park, M. Batuwangala, J. Bill, M. Sitti, Cancer cells biomineralize ionic gold into nanoparticles-microplates via secreting defense proteins with specific gold-binding peptides. Acta Biomater. **71**, 61–71 (2018). doi:https://doi.org/10.1016/j.actbio.2018.02.022

A.V. Singh, V. Chandrasekar, P. Janapareddy, D.E. Mathews, P. Laux, A. Luch, Y. Yang, B. Garcia-Canibano, S. Balakrishnan, J. Abinahed, A. Al Ansari, S.P. Dakua, Emerging Application of Nanorobotics and Artificial Intelligence To Cross the BBB: Advances in Design, Controlled Maneuvering, and Targeting of the Barriers. ACS Chem. Neurosci. **12**, 1835–1853 (2021). doi:https://doi.org/10.1021/acschemneuro.1c00087

G. Sriram, U.T. Uthappa, R.M. Rego, M. Kigga, T. Kumeria, H.-Y. Jung, M.D. Kurkuri, Ceria decorated porous diatom-xerogel as an effective adsorbent for the efficient removal of Eriochrome Black T. Chemosphere **238**, 124692 (2020). doi:https://doi.org/10.1016/j.chemosphere.2019.124692

Y. Su, N. Lundholm, M. Ellegaard, Effects of abiotic factors on the nanostructure of diatom frustules—ranges and variability. Appl. Microbiol. Biotechnol. **102**, 5889–5899 (2018). doi:https://doi.org/10.1007/s00253-018-9087-1

E. Sulman, V. Doluda, S. Dzwigaj, E. Marceau, L. Kustov, O. Tkachenko, A. Bykov, V. Matveeva, M. Sulman, N. Lakina, Catalytic properties of Ru nanoparticles introduced in a matrix of hypercrosslinked polystyrene toward the low-temperature oxidation of d-glucose. J. Mol. Catal. A: Chem. **278**, 112–119 (2007). doi:https://doi.org/10.1016/j.molcata.2007.08.029

U.T. Uthappa, M. Kigga, G. Sriram, K.V. Ajeya, H.-Y. Jung, G.M. Neelgund, M.D. Kurkuri, Facile green synthetic approach of bio inspired polydopamine coated diatoms as a drug vehicle for controlled drug release and active catalyst for dye degradation. Microporous Mesoporous Mater. **288**, 109572 (2019). doi:https://doi.org/10.1016/j.micromeso.2019.109572

U.T. Uthappa, G. Sriram, V. Brahmkhatri, M. Kigga, H.-Y. Jung, T. Altalhi, G.M. Neelgund, M.D. Kurkuri, Xerogel modified diatomaceous earth microparticles for controlled drug release studies. New J. Chem. **42**, 11964–11971 (2018a). doi:https://doi.org/10.1039/C8NJ01238E

U.T. Uthappa, G. Sriram, O.R. Arvind, S. Kumar, J. Ho Young, G.M. Neelgund, D. Losic, M.D. Kurkuri, Engineering MIL-100(Fe) on 3D porous natural diatoms as a versatile high performing platform for controlled isoniazid drug release, Fenton's catalysis for malachite green dye degradation and environmental adsorbents for Pb2 + removal and dyes. Appl. Surf. Sci. **528**, 146974 (2020). doi:https://doi.org/10.1016/j.apsusc.2020.146974

U.T. Uthappa, V. Brahmkhatri, G. Sriram, H.-Y. Jung, J. Yu, N. Kurkuri, T.M. Aminabhavi, T. Altalhi, G.M. Neelgund, M.D. Kurkuri, Nature engineered diatom biosilica as drug delivery systems. J. Controlled Release **281**, 70–83 (2018b). doi:https://doi.org/10.1016/j.jconrel.2018.05.013

D. Vona, S.R. Cicco, R. Ragni, G. Leone, M. Lo Presti, G.M. Farinola, Biosilica/polydopamine/silver nanoparticles composites: new hybrid multifunctional heterostructures obtained by chemical modification of Thalassiosira weissflogii silica shells. MRS Commun. **8**, 911–917 (2018). doi:https://doi.org/10.1557/mrc.2018.103

D. Wisser, S.I. Brückner, F.M. Wisser, G. Althoff-Ospelt, J. Getzschmann, S. Kaskel, E. Brunner, 1H–13 C–29Si triple resonance and REDOR solid-state NMR—A tool to study interactions between biosilica and organic molecules in diatom cell walls. Solid State Nucl. Magn. Reson. **66–67**, 33–39 (2015). doi:https://doi.org/10.1016/j.ssnmr.2014.12.007

X. Yan, J. Meng, X. Hu, R. Feng, M. Zhou, Synthesis of thiol-functionalized mesoporous silica nanoparticles for adsorption of Hg2 + from aqueous solution. J. Solgel Sci. Technol. **89**, 617–622 (2019). doi:https://doi.org/10.1007/s10971-019-04923-6